Diagonal patterns and chevron effect in intersecting traffic flows

J. Cividini, C. Appert-Rolland, and H.J. Hilhorst

Laboratory of Theoretical Physics, CNRS (UMR 8627),
University Paris-Sud, Bâtiment 210, F-91405 Orsay Cedex, France

We study a lattice model of two perpendicular intersecting flows of pedestrians represented by hard core particles of two types, eastbound ('$\mathcal{E}$') and northbound ('$\mathcal{N}$'). Each flow takes place on a strip of width M so that the intersection is an $M \times M$ square lattice. In experiment and simulation there occurs on this square spontaneous formation of a diagonal pattern of alternating $\mathcal{E}$ and $\mathcal{N}$ particles. By a linear stability analysis of the corresponding mean-field equations we point out the origin of this pattern formation phenomenon. A refined investigation reveals that for large enough M the pattern actually consists of chevrons rather than straight diagonals. We provide an explanation for this chevron effect.

PACS numbers: 05.65.+b, 45.70.Vn, 89.75.Kd

Pedestrian motion in dense environments is of much theoretical and practical interest [1, 2]. Instances of applications are shopping streets, waiting lines, crowds that enter or leave a room, converge to a stadium, participate in a demonstration, and so on. Simplified models help us understand the behavior of individuals under such circumstances as well as the collective behavior that results from it. They may also have more general applicability than the question that initially prompted their formulation.

The present investigation was motivated by the experimental observation [3] of an instability that occurs at the intersection of two perpendicular unidirectional flows of pedestrians: Walkers segregate into a pattern of approximate diagonals of walkers of the same type. In a variety of models simulating crossing flows (agent based [4, 5], PDEs [5], BML [7]) it has been remarked that such patterns occur, but the formation mechanism has not been systematically studied. In this paper we tackle this question with combined numerical and theoretical approaches. First, we explain the pattern formation instability both for closed and open systems. Moreover, we show that superposed on the instability there is a subtle 'chevron effect', whose origin we explain. This effect, which so far has not been observed, may be expected to be visible under favorable circumstances.

We model a street of width M as a set of M parallel one-dimensional lattices or 'lanes' [8]. Two intersecting one-way streets lead to the geometry of Fig. 1, which has the $(1, 1)$ diagonal through the origin as an axis of symmetry. Eastbound (or '$\mathcal{E}$') and northbound (or '$\mathcal{N}$') particles are injected into each lane at some large distance L from the intersection square with a probability α per time step. This probability determines the incoming current $J(\alpha)$ in each lane [6]. For moving the particles we choose for convenience the frozen shuffle update [9]. It will appear that the phenomena of interest are independent of the details of the update mechanism. Under frozen shuffle update, during a unit interval all particles are visited in a fixed sequence and each one executes a move unless its target site is occupied; that is, the particles move ballistically unless blocked. Particles entering the system are randomly inserted in the update sequence and those exiting are deleted from it. Blocking may happen to a particle either in the intersection square itself or in the street segments leading up to it. In the simulations we chose L (see Fig. 1) larger than the lengths of any waiting lines observed at the entrance, so that effectively $L = \infty$. We therefore have a simple model depending only on the two parameters α and M, whose interest as an example of a driven nonequilibrium system goes, we believe, beyond the present application. Simulations were carried out for intersecting streets of widths up to $M = 640$. The pattern formation studied here appears in the so-called *free flow phase* ($\alpha \lesssim 0.10$ for the M values concerned), in which in each lane the current exiting the intersection is equal to $J(\alpha)$. We will stay away from higher values of α, where jamming transitions are known to occur [8, 10].

For $t > 0$ particles start entering the initially empty intersection square. After a number of time steps typically no larger than a few times the linear lattice size M, the occupation of the intersection square reaches a stationary state. We observed that this state has the following properties.

(i) There is an α dependent penetration length $\xi(\alpha)$, such that for $M \lesssim \xi$ the occupation of the intersection square appears disordered to the eye. For $\alpha = 0.09$ the penetration length equals $\xi(\alpha) \approx 50$; for $\alpha \to 0$ it diverges.

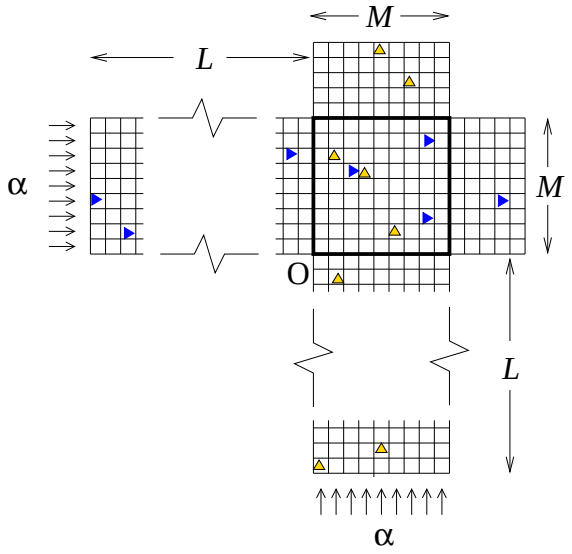

FIG. 1: Intersection of two one-way streets of width M. The blue particles (▶) move eastward and the orange particles (▲) northward. The parameter α determines the particle injection rate. The region bordered by the heavy solid line is the 'intersection square'.

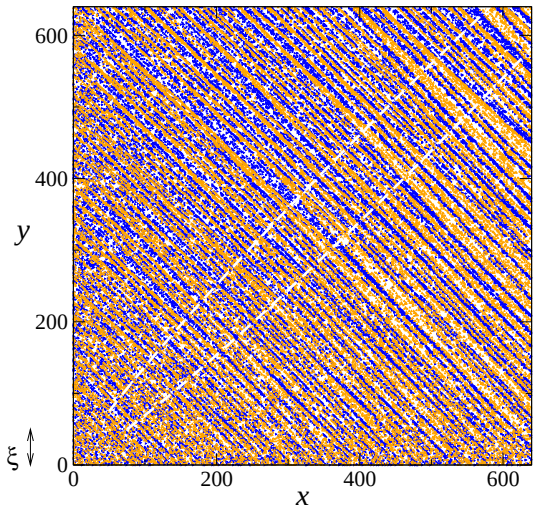

FIG. 2: Typical configuration of the intersection square in the stationary state for $M = 640$ and $\alpha = 0.09$. The orange particles arrive from the left and the blue ones from the bottom. Between the lower-left and the upper-right, the particles self-organize to form a diagonal pattern. The dashed white lines delimit different regions discussed in the text.

(ii) For $M \gtrsim \xi$ alternating stripes of $\mathcal{E}$ and $\mathcal{N}$ particles parallel to the $(1,-1)$ direction begin to be distinguishable. For $M \gg \xi$ they are clearly visible, as may be seen from Fig. 2, where $M = 640$ and $\alpha = 0.09$. Although the striped pattern never becomes fully regular, its wavelength is typically in the range from 5 to 15 lattice distances. This organization into stripes decreases the probability for a particle to be blocked below its value for a random particle distribution, and therefore increases the particles' average velocity.

(iii) Closer examination of Fig. 2 reveals an effect just barely visible to the eye: the angle θ of the striped pattern (as measured clockwise from the west) is *not exactly equal to* 45° but deviates from it by an amount $\Delta\theta(\mathbf{r})$, where $\mathbf{r} = (x, y)$ denotes the position in space. Although small (of the order of a degree), the deviation $\Delta\theta(\mathbf{r})$ may be measured [12] unambiguously in the neighborhood of any site $\mathbf{r}$. It is negative above the axis of symmetry and positive below it.

(iv) In the upper (lower) triangular region delimited by the dashed white lines in Fig. 2, the deviation $\Delta\theta(\mathbf{r})$ is close to a constant $\mp\Delta\theta_0$. This confers to the stripes the appearance of chevrons, and we will speak of the 'chevron effect'. The tips of the chevrons, located in the transition zone between the two white lines, are rounded. Empirically we find $\Delta\theta_0(\alpha) \simeq c\alpha$ with $c \approx 15°$.

We will now first explain the stripe formation instability and then return to the chevron effect.

Let us denote by $\rho_t^{\mathcal{E},\mathcal{N}}(\mathbf{r})$ the particle densities of the $\mathcal{E},\mathcal{N}$ particles on site $\mathbf{r}$ after t time steps. In an exact description of the time evolution the $\rho_t^{\mathcal{E},\mathcal{N}}(\mathbf{r})$ would couple higher order correlations. Breaking these, we postulate the mean-field equations

$$\begin{aligned}\rho_{t+1}^{\mathcal{E}}(\mathbf{r}) &= [1-\rho_t^{\mathcal{N}}(\mathbf{r})]\rho_t^{\mathcal{E}}(\mathbf{r}-\boldsymbol{e}_x) + \rho_t^{\mathcal{N}}(\mathbf{r}+\boldsymbol{e}_x)\rho_t^{\mathcal{E}}(\mathbf{r}),\\ \rho_{t+1}^{\mathcal{N}}(\mathbf{r}) &= [1-\rho_t^{\mathcal{E}}(\mathbf{r})]\rho_t^{\mathcal{N}}(\mathbf{r}-\boldsymbol{e}_y) + \rho_t^{\mathcal{E}}(\mathbf{r}+\boldsymbol{e}_y)\rho_t^{\mathcal{N}}(\mathbf{r}),\end{aligned} \tag{1}$$

where $\boldsymbol{e}_{x,y}$ are basis vectors. Eqs. (1) take into account the interactions between particles of different type ($\mathcal{E}$ and $\mathcal{N}$) but neglect those between particles of the same type. This may be justified by the fact [12] that in the low density limit the frequency of $\mathcal{E}/\mathcal{N}$ and $\mathcal{N}/\mathcal{E}$ blocking events is $\sim \overline{\rho}^2$, whereas that of same-particle blocking is $\sim \overline{\rho}^3$, where $\overline{\rho}$ is the average density of each of the two particle types in the intersection.

As a first step we impose toroidal boundary conditions on (1) and perform a linear stability analysis around a uniform initial state. Let $\rho_t^{\mathcal{E},\mathcal{N}}(\mathbf{r}) = \overline{\rho} + \delta\rho_t^{\mathcal{E},\mathcal{N}}(\mathbf{r})$, where $\overline{\rho}$ now replaces α as the control parameter and the $\delta\rho_t^{\mathcal{E},\mathcal{N}}(\mathbf{r})$ are small. In terms of the Fourier transforms $\delta\hat{\rho}_t^{\mathcal{E},\mathcal{N}}(\mathbf{q})$

with $\mathbf{q} = (q_x, q_y)$ the linearized equations read

$$\begin{pmatrix} \delta\hat{\rho}^{\mathcal{E}}_{t+1}(\mathbf{q}) \\ \delta\hat{\rho}^{\mathcal{N}}_{t+1}(\mathbf{q}) \end{pmatrix} = \begin{pmatrix} \mathrm{e}^{\mathrm{i}q_x} R_{q_x} & R_{q_x} - 1 \\ R_{q_y} - 1 & \mathrm{e}^{\mathrm{i}q_x} R_{q_y} \end{pmatrix} \begin{pmatrix} \delta\hat{\rho}^{\mathcal{E}}_{t}(\mathbf{q}) \\ \delta\hat{\rho}^{\mathcal{N}}_{t}(\mathbf{q}) \end{pmatrix}, \tag{2}$$

where $R_q = 1 + \overline{\rho}(\mathrm{e}^{-\mathrm{i}q} - 1)$. The larger eigenvalue of the 2×2 matrix in (2) has an absolute value whose maximum, located on the diagonal $q_x = q_y$, exceeds unity; it is associated with an unstable mode traveling in the $(1, 1)$ direction and having the wavelength $\lambda_{\max} = 2\pi/q_{\max} = 6[1 - (\sqrt{3}/\pi)\overline{\rho}]$. This calculation therefore explains the formation of a diagonal striped pattern as a consequence of unstable Fourier modes present in the initial state.

The nonlinear regime is outside of the reach of this analysis; however, numerical solution of the nonlinear equations (1), still with toroidal boundary conditions, shows that the solution tends to a stationary state consisting of stripes with alternatingly only $\rho^{\mathcal{E}}_t(\mathbf{r}) \neq 0$ or only $\rho^{\mathcal{N}}_t(\mathbf{r}) \neq 0$, and separated by unoccupied sites in such a way that the nonlinear terms in (1) vanish at all times. The density profiles $\rho^{\mathcal{E},\mathcal{N}}_t(\mathbf{r})$ then advance unaltered eastward and northward around the torus, respectively, with unit velocity.

In the original crossing street system the interaction square has open west and south boundaries that are subject to time-dependent boundary noise. It is therefore necessary to show that this noise excites unstable modes analogous to those found above for the torus. For the open system we consider the nonlinear equations (1) with the stochastic boundary conditions

$$\begin{aligned} \rho^{\mathcal{E}}_t(0, k) &= \eta^{\mathcal{E}}_t(k), \qquad & \rho^{\mathcal{N}}_t(k, 0) &= \eta^{\mathcal{N}}_t(k), \\ \rho^{\mathcal{E}}_t(M+1, k) &= 0, \qquad & \rho^{\mathcal{N}}_t(k, M+1) &= 0, \end{aligned} \tag{3}$$

for all $k = 1, 2, \ldots, M$, where the $\eta^{\mathcal{E},\mathcal{N}}_t(k)$ are i.i.d. random variables of average $\overline{\eta}$ and which we take from a uniform distribution on $[\frac{1}{2}\overline{\eta}, \frac{3}{2}\overline{\eta}]$. Here $\overline{\eta}$ replaces α as the control parameter. The initial condition is arbitrary.

After linearizing these equations we found, at the cost of considerable algebra, their Green function [13] and established the existence of unstable modes propagating in the $(1, 1)$ direction. This completes our explanation of the origin of the pattern formation instability.

We now turn to the chevron effect. In the linear stability analysis of (1) with the stochastic boundary conditions (3) this effect does not appear. However, numerical resolution of the full nonlinear equations (1) with (3) leads to the same chevron effect as simulation of the particle system. This is one more strong indication that it must exist for a wide class of time evolution rules, as long as these incorporate the basic ingredient of repulsion between two unidirectionally and perpendicularly traveling particle types.

We now present further observations made on our simulation of the particle system, which will help us explain the chevron effect.

(v) The stripes of the $\mathcal{E}$ and those of the $\mathcal{N}$ particles move almost without any mutual penetration.

This is compatible with an inclination θ of the stripe direction only if $\tan\theta(\mathbf{r}) = v^{\mathcal{N}}(\mathbf{r})/v^{\mathcal{E}}(\mathbf{r})$, where $v^{\mathcal{E},\mathcal{N}}$ is the time-averaged velocity of the $\mathcal{E}, \mathcal{N}$ particles on site $\mathbf{r}$. Now the boundary conditions impose the same stationary current J in each lane, so that $J = \rho^{\mathcal{E}}(\mathbf{r})v^{\mathcal{E}}(\mathbf{r}) = \rho^{\mathcal{N}}(\mathbf{r})v^{\mathcal{N}}(\mathbf{r})$ with $\rho^{\mathcal{E},\mathcal{N}}(\mathbf{r})$ the time-averaged densities. Combined with the preceding equation for $\tan\theta(\mathbf{r})$ this yields

$$\tan\theta(\mathbf{r}) = \rho^{\mathcal{E}}(\mathbf{r})/\rho^{\mathcal{N}}(\mathbf{r}). \tag{4}$$

It follows from (4) that $\Delta\theta(\mathbf{r}) \neq 0$ requires $\rho^{\mathcal{E}}(\mathbf{r})$ and $\rho^{\mathcal{N}}(\mathbf{r})$ to be different. We have verified that relation (4) is satisfied in good approximation both in the simulations of the particle system and in the numerical solution of (1) with (3), in the two triangular regions as well as in the transition zone between them. We remark parenthetically that since $\Delta\theta$ is small, the difference between the two densities is small as well. Indeed, a particle simulation for $M = 500$ and with current $J(\alpha) = 0.06$ yields in the upper triangular region $\rho^{\mathcal{E}} \approx 0.0606$ and $\rho^{\mathcal{N}} \approx 0.0621$. This establishes the general consistency of the picture, still without explaining it.

(vi) Next we refer to the zoom, shown in Fig. 3, on an area located in the upper triangular region of Fig. 2. We observe that in this region the stripes of the $\mathcal{N}$ particles are dense, whereas those of the $\mathcal{E}$ particles are sparse. A consequence, visible even if barely so, is that the upper triangular region in Fig. 2 looks bluish and the lower triangle more orange-like. The asymmetry observed here between the two particle types will offer the clue to understand the chevron effect.

The core of the problem is to show the existence of modes of propagation having stripe angles different from 45°. Let us consider what happens near the entrance boundary of the $\mathcal{E}$ particles, that is, for $x \approx \xi$ but $y \gg \xi$. Near this boundary the $\mathcal{E}$ particles (▶), having entered the intersection square randomly, fill the space offered to them between the $\mathcal{N}$ stripes (▲) also largely randomly. This suggests to consider the special class of $\mathcal{N}$ stripes of which an example is shown in Fig. 4a. The stripes consist of straight segments at an angle of 45°, connected by 'kinks' such as the one that occurs in Fig. 4a at the level of particle B, and that is associated with the presence of the eastbound particle A. The other $\mathcal{E}$ particles in Fig. 4a occupy random positions. In order to facilitate the analysis we now invoke the irrelevance of the details

of the time evolution rules. This allows us to employ in the present argument the alternated parallel update: at each time step first all $\mathcal{E}$ particles move simultaneously (unless blocked) and then all unblocked $\mathcal{N}$ particles do so.

When this update procedure is applied to the configuration of Fig. 4a, we see that during the $(t+1)$th time step none of the eastbound particles is blocked; in particular, A and C move and block B and D, respectively. As a result the kink associated with A moves one step to the right along the northbound stripe, and C creates a new kink at the beginning of the stripe, at the level of particle D. (see Fig. 4b). In the next time steps particles A and C will both travel from left to right along the stripe, each of them taking its associated kink along, and the connected structure of the stripe will be preserved.

If the set of kinks has a linear density $\rho_{\rm kink}$ along the stripe, the average stripe angle θ will be given by $\tan\theta = 1 - \rho_{\rm kink}$. Since $\rho_{\rm kink}$ also represents the fraction of blocked moves of the $\mathcal{N}$ particles, the stripe's speed will be $v^{\mathcal{N}} = 1 - \rho_{\rm kink}$. Hence we have demonstrated the most distinctive ingredient of the chevron effect: the existence of a nonlinear mode consisting of a stripe with an average slope different from 45°, that propagates at an average speed $v^{\mathcal{N}} < 1$.

We must expect similar modes to be present for a wide class of time evolution rules, including those of the original particle system with frozen shuffle update, and those of Eqs. (1); for both of these the explicit analysis would, however, be much more difficult. Of course quantitatives features such as the exact value of $\Delta\theta$ or the wavelength of the pattern will depend on the specificity of the time evolution rules.

Returning to the example of Fig. 4 we note that a uniformly random spatial distribution of the $\mathcal{E}$ particles would lead to $\rho_{\rm kink} = \rho^{\mathcal{E}}$, and that $v^{\mathcal{E}} = 1$. Combining these approximations we are led to a fully explicit expression for the angle, namely $\tan\theta = 1 - J$, in which $J(\alpha)$ is known [6]. Since a correlated distribution of the $\mathcal{E}$ particles would lead to a lower $\rho_{\rm kink}$, we expect that this formula, while giving the correct order of magnitude, overestimates the inclination. Indeed, for $J = 0.06$ it yields $\Delta\theta_0 = 1.8°$, to be compared to 0.7° obtained via Eq. (4) and 0.9° from direct measurement, both in a frozen shuffle update simulation.

We have presented a set of simulation results, numerical work, and analytic work that coherently bring out a pattern formation instability accompanied by a subtle but unmistakable 'chevron' effect, quantified by an angular deviation $\Delta\theta(\mathbf{r})$ of the pattern. The effect may be measured in the simulation and also calculated numerically. Determining the precise values of the time-averaged density profiles $\rho^{\mathcal{E},\mathcal{N}}(\mathbf{r})$ of the two intersecting particle flows, and thence of the preferred angle of inclination $\Delta\theta(\mathbf{r})$, is still an open question. Its solution might require a hydrodynamic approach to this problem, which however is beyond the scope of this communication. In any case, we expect the chevron effect to be generic for a wide class of transport problems, including those of Refs. [4, 5, 7], that share the features of intersecting unidirectional flows. Because of its smallness, observing the effect in an experiment or in a real-life traffic situation will not be easy, but must be anticipated.

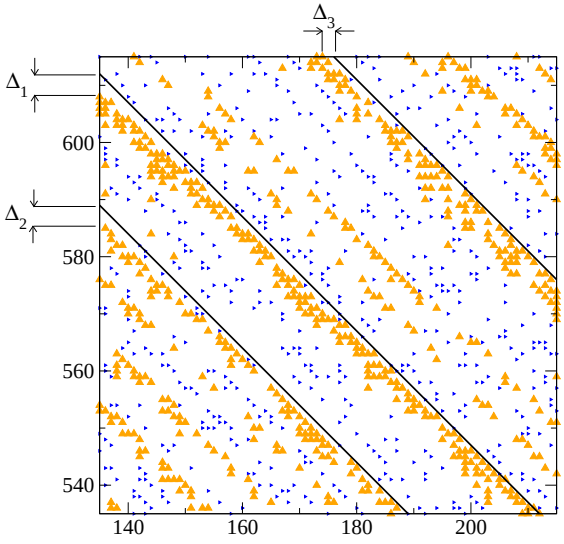

FIG. 3: Zoom on a region of Fig. 2. To emphasize their difference the northbound particles (▲) have been indicated by larger symbols than the eastbound particles (▶). The black solid lines are at an angle of 45°. The nonzero distances Δ_1, Δ_2, and Δ_3 show that locally $\Delta\theta(\mathbf{r}) < 0$.

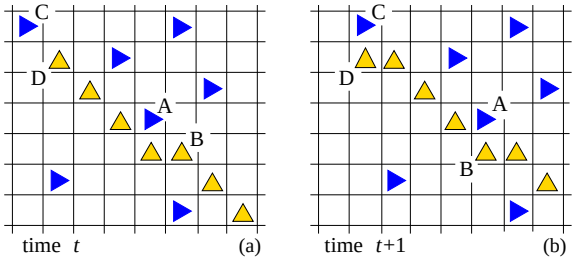

FIG. 4: Mechanism causing the deviation $\Delta\theta$ of a stripe of northbound particles (▲) in the upper triangular region.

[1] A. Schadschneider, Modelling of transport and traffic problems, in: H. Umeo, S. Morishita, K. Nishinari, T. Komatsuzaki, S. Bandini (Eds.), Cellular automata, Proceedings. Book Series: Lecture Notes in Computer Science, Vol. 5191, 2008, pp. 22–31.

[2] D. Helbing, Traffic and related self-driven many-particle systems, Reviews of Modern Physics 73 (2001) 1067–1141.

[3] S. P. Hoogendoorn, W. Daamen, Self-organization in walker experiments, in: S. Hoogendoorn, S. Luding, P. Bovy, et al. (Eds.), Traffic and Granular Flow '03, Springer, 2005, p. 121–132

[4] S. P. Hoogendoorn, P. H. L. Bovy, Simulation of pedestrian flows by optimal control and differential games, Optim. Control Appl. Meth. 24 (2003) 153–172.

[5] K. Yamamoto, M. Okada, Continuum model of crossing pedestrian flows and swarm control based on temporal/spatial frequency, in: 2011 IEEE International Conference on Robotics and Automation, 2011.

[6] With the frozen shuffle update of this paper the exact formula is $J(\alpha) = -\log(1-\alpha)/[1-\log(1-\alpha)]$.

[7] O. Biham, A. A. Middleton, D. Levine, Self-organization and a dynamic transition in traffic-flow models, Phys. Rev. A 46 (1992) R6124–R6127.

[8] H.J. Hilhorst, C. Appert-Rolland, A multi-lane TASEP model for crossing pedestrian traffic flows, J. Stat. Mech. (2012) P06009.

[9] C. Appert-Rolland, J. Cividini, H.J. Hilhorst, Frozen shuffle update for an asymmetric exclusion process on a ring, J. Stat. Mech. (2011) P07009.

[10] C. Appert-Rolland, J. Cividini, H.J. Hilhorst, Intersection of two tasep traffic lanes with frozen shuffle update, J. Stat. Mech. (2011) P10014.

[11] C. Appert-Rolland, J. Cividini, H.J. Hilhorst, Frozen shuffle update for a deterministic totally asymmetric simple exclusion process with open boundaries, J. Stat. Mech. (2011) P10013.

[12] J. Cividini, H.J. Hilhorst, C. Appert-Rolland, In preparation.

[13] J. Cividini, H.J. Hilhorst, In preparation.